INSTITUT DE FRANCE
Académie des sciences

Comptes Rendus

Chimie

Amira K. Hajri, Marzough A. Albalawi, Nadia H. Elsayed and Faouzi Aloui

Synthesis and photophysical properties of new reactive fluorophenanthrenes

Volume 23, issue 4-5 (2020), p. 315-327

Published online: 23 September 2020
Issue date: 10 November 2020

https://doi.org/10.5802/crchim.29

Les Comptes Rendus. Chimie *sont membres du*
Centre Mersenne pour l'édition scientifique ouverte
www.centre-mersenne.org
e-ISSN : 1878-1543

Comptes Rendus
Chimie
2020, 23, nº 4-5, p. 315-327
https://doi.org/10.5802/crchim.29

Full paper / *Mémoire*

Synthesis and photophysical properties of new reactive fluorophenanthrenes

Synthèse et propriétés photophysiques de nouveaux fluorophénanthrènes réactifs

Amira K. Hajri [a, b], Marzough A. Albalawi [a], Nadia H. Elsayed [a, c] and Faouzi Aloui [*, b]

[a] Department of Chemistry, Alwajh College, University of Tabuk, KSA

[b] University of Monastir, Faculty of Sciences, Laboratory of Asymmetric Synthesis and Molecular Engineering of Materials for Electronic Organics (LR18ES19), 5019 Monastir, Tunisia

[c] Department of Polymers and Pigments, National Research Centre, Cairo 12311, Egypt

E-mails: ahejari@ut.edu.sa (A. K. Hajri), maalbalawi@ut.edu.sa (M. A. Albalawi), nhussein@ut.edu.sa (N. H. Elsayed), aloui.faouzi@laposte.net (F. Aloui)

Abstract. A series of six new suitably functionalized fluorophenanthrene derivatives were synthesized through a simple procedure, making use of inexpensive starting materials under mild conditions. The target phenanthrenes were characterized by ^{1}H and ^{13}C NMR and FT-IR spectroscopies. UV–Vis absorption and photoluminescence of these phenanthrenes were evaluated in solutions. A notable behavior and a strong fluorescence in the blue region of the visible spectrum were observed, making them potential candidates for organic light-emitting diode technology or advanced materials. Their electrochemical behavior was also experimentally examined in solution, demonstrating an important charge transfer interaction owing to their π-conjugated electronic system.

Résumé. Une série de six nouveaux dérivés de fluorophénanathrène convenablement fonctionnalisés ont été synthétisés selon une procédure simple utilisant des réactifs peu coûteux dans des conditions douces. Les phénanthrènes cibles ont été caractérisés par RMN ^{1}H et ^{13}C et IR à transformée de Fourrier. L'étude de l'absorption UV–Vis et de la photoluminescence de ces phénanthrènes a été évaluée en solution montrant un comportement notable et une forte fluorescence dans la région bleue du spectre visible, ce qui permet de les considérer comme des candidats potentiels pour la technologie OLED ou des matériaux avancés. Leur comportement électrochimique a été aussi examiné expérimentalement en solution démontrant une interaction de transfert de charge importante grâce à leur système électronique π-conjugué.

Keywords. Phenanthrene, Photo-oxidation, UV–Vis absorption, Photoluminescence, Cyclic voltammetry.

Mots-clés. Phénanthrène, Photooxydation, Absorption UV–Vis, Photoluminescence, Voltammétrie cyclique.

[*] Corresponding author.

Manuscript received 16th March 2020, revised and accepted 29th April 2020.

1. Introduction

Phenanthrenes are representative π-conjugated polyaromatic compounds consisting of three *ortho*-fused benzenoid units. They are considered interesting materials for photoluminescent applications [1, 2]. They are known to exhibit good electrical and optical properties due to their unique photoluminescence (PL) and electroluminescence properties [3–7] and their ease of use in the fabrication of new sensors or nanostructured materials. Among other distinctive properties of phenanthrenes are their higher thermal stability, lower toxicity than other polyaromatic systems, and their ready functionalization, which make them very desirable for applications in materials science [8–10].

Indeed, the synthesis of phenanthrene derivatives with important properties has been attracting attention in the manufacture of new materials, opening up new fields of potential applications. Inspired by the literature, many phenanthrene derivatives have been synthesized, and their photophysical and thermal properties including their electrochemistry have been intensively studied. These derivatives offer access to various organic devices such as organic light-emitting diodes (OLEDs) [11–18], solar cells [19–21], superconductors [22,23], etc. In an independent study, Zhang and co-workers reported the synthesis of phenanthro-imidazole **1** (Figure 1) and used it for OLEDs [24]. More recently, Akula and coworkers have reported the synthesis of ruthenium complex **2**, revealing good optical, electrochemical, and thermal properties, which has been used as a promising electron-transport material for organic solar cells [25].

Phenanthrene derivatives are important molecules exhibiting interesting properties and have been attracting interest not only for their applications as organic materials but also for their versatile synthetic route. Up until now, various strategies have been applied for producing these π-conjugated systems. One of the most widely employed methods is the photocyclization approach, which is considered fast, economical, and practical. In addition, using this method, it is easy to obtain new electron-rich structured phenanthrenes with a wide range of characterizations and applications.

2. Experimental section

2.1. *General*

The majority of the experiments were performed under anhydrous conditions (dry N_2 or Ar) using freshly distilled solvents. Solvents and starting materials were purchased from Aldrich. Column chromatography purifications were performed over silica gel obtained from SiliCycle chemical division (40–63 nm; 230–240 mesh). Photochemical reactions were carried out using a 150 W mercury lamp. ^{1}H and ^{13}C NMR spectra were recorded on a Bruker AM 300, using $CDCl_3$ and DMSO-d_6 as deuterated solvents with tetramethylsilane as the internal reference at room temperature. Chemical shifts (δ) were reported in parts per million (ppm) relatively to tetramethylsilane. Multiplicity was reported as follows: s: singlet, d: doublet, dd: doublet of doublets, and m: multiplet. UV–Vis spectroscopy was recorded on a Varian Cary 5000 spectrometer in quartz cuvettes with a path length of 1 cm. Electrochemical studies were carried out under argon atmosphere using an Eco Chemie Autolab PGSTAT 30 potentiostat for voltammetric measurements, connected to a conventional three-electrode cell. The working electrode was a platinum microdisk, the reference electrode was a saturated calomel electrode (SCE), and the counter-electrode was a platinum wire.

2.2. *General procedure for the synthesis of α,β-unsaturated nitriles **2a–f***

In a two-neck, 100-mL flask placed under argon, 4.5 mmol (1 eq) of p-fluorophenylacetonitrile (**1**), 4.5 mmol (1 eq) of aromatic aldehyde, and 30 mL of anhydrous methanol were introduced. The mixture was stirred until total dissolution of the reagents. Then 375 mg of sodium methanolate (8.3 mmol, 2 eq) was added in small portions, and the mixture was stirred at room temperature. The evolution of the reaction was monitored by TLC. The resulting product was recovered by filtration on a sintered glass, washed with cold methanol and then with distilled water, and dried.

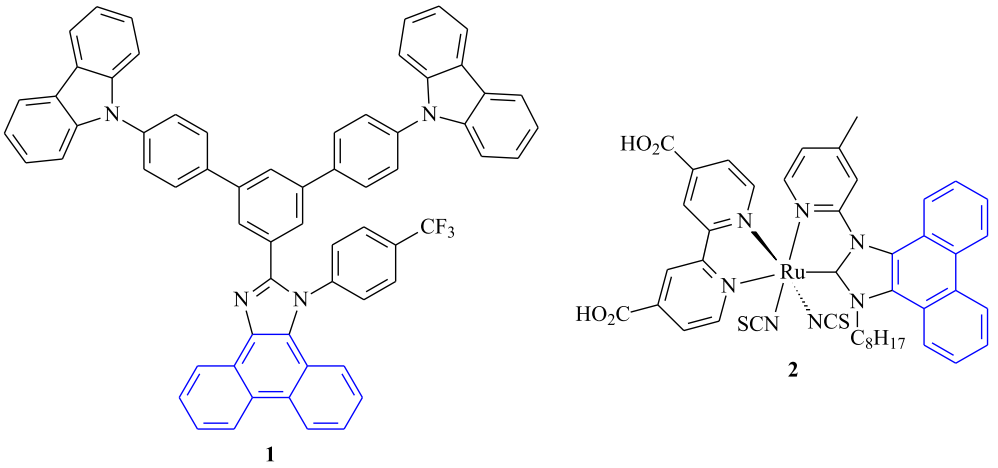

Figure 1. Phenanthrene derivatives **1** and **2** as promising materials.

2.2.1. *(Z)-2-(p-fluorophenyl)-3-(p-methoxyphenyl) acrylonitrile (**2a**)*

White solid, 85%; m.p. = 97–99 °C; ^{1}H NMR (300 MHz, $CDCl_3$): δ (ppm): 3.87 (s, 3H, OCH_3), 6.97 (d, J = 9 Hz, 2H), 7.09–7.15 (m, 2H), 7.39 (s, 1H), 7.60–7.65 (m, 2H), 7.86 (d, J = 9 Hz, 2H); ^{13}C NMR (75 MHz, $CDCl_3$): δ (ppm): 54.91 (OCH_3), 107.22 (C), 113.95 (2CH), 115.37 (d, $J_{C\text{-}F}$ = 21.8 Hz, 2CH), 117.83 (CN), 125.90 (C), 127.05 (d, $J_{C\text{-}F}$ = 8.2 Hz, 2CH), 130.30 (C), 130.61 (2CH), 141.25 (CH), 161.04 (C–O), 162.48 (d, $J_{C\text{-}F}$ = 251.2 Hz, CF); ^{19}F NMR (282 MHz, $CDCl_3$): δ (ppm): −111.6 Hz (s, F).

2.2.2. *(Z)-3-(p-bromophenyl)-2-(p-fluorophenyl) acrylonitrile (**2b**)*

Yellow solid, 80%; m.p. = 88–90 °C; ^{1}H NMR (300 MHz, $CDCl_3$): δ (ppm): 7.12–7.17 (m, 2H), 7.39 (s, 1H), 7.59–7.67 (m, 4H), 7.73 (d, J = 8.7 Hz, 2H); ^{13}C NMR (75 MHz, $CDCl_3$): δ (ppm): 110.97 (C), 115.58 (d, $J_{C\text{-}F}$ = 21.9 Hz, 2CH), 117.01 (CN), 124.45 (C), 127.36 (d, $J_{C\text{-}F}$ = 8.2 Hz, 2CH), 129.89 (C), 129.93 (2CH), 131.76 (2CH), 131.96 (C), 140.06 (CH), 161.22 (d, $J_{C\text{-}F}$ = 249 Hz, CF); ^{19}F NMR (282 MHz, $CDCl_3$): δ (ppm): −111.13 Hz (s, F).

2.2.3. *(Z)-4-(2-cyano-2-(p-fluorophenyl)vinyl) benzonitrile (**2c**)*

White solid, 65%; m.p. = 208–210 °C; ^{1}H NMR (300 MHz, $CDCl_3$): δ (ppm): 7.17–7.22 (m, 2H), 7.50 (s, 1H), 7.71 (d, J = 8.1 Hz, 2H), 7.77 (d, J = 7.8 Hz, 2H), 7.97 (d, J = 7.8 Hz, 2H), ^{13}C NMR (75 MHz, $CDCl_3$): δ (ppm): 113.13 (C), 113.79 (C), 115.82 (d, $J_{C\text{-}F}$ = 22.1 Hz, 2CH), 116.55 (CN), 117.71 (CN), 127.67 (d, $J_{C\text{-}F}$ = 8.4 Hz, 2CH), 129.05 (2CH), 132.20 (2CH), 137.18 (C), 138.80 (CH), 161.55 (d, $J_{C\text{-}F}$ = 252 Hz, CF); ^{19}F NMR (282 MHz, $CDCl_3$): δ (ppm): −109.85 (s, F).

2.2.4. *(Z)-2,3-bis(p-fluorophenyl)acrylonitrile (**2d**)*

White solid, 90%; m.p. = 173–175 °C; ^{1}H NMR (300 MHz, $CDCl_3$): δ (ppm): 7.14–7.21 (m, 4H), 7.44 (s, 1H), 7.64–7.69 (m, 2H), 7.88–7.93 (m, 2H); ^{13}C NMR (75 MHz, $CDCl_3$): δ (ppm): 110.00 (C), 115.53 (d, $J_{C\text{-}F}$ = 21.7 Hz, 4CH), 117.19 (CN), 127.29 (d, $J_{C\text{-}F}$ = 8.2 Hz, 2CH), 129.36 (C), 130.01 (C), 130.74 (d, $J_{C\text{-}F}$ = 9 Hz, 2CH), 140.19 (CH), 161.13 (d, $J_{C\text{-}F}$ = 248.2 Hz, CF), 161.61 (d, $J_{C\text{-}F}$ = 252 Hz, CF); ^{19}F NMR (282 MHz, $CDCl_3$): δ (ppm): −109.47 (s, F).

2.2.5. *(Z)-2-(p-fluorophenyl)-3-(3′,4′-dimethoxyphenyl)acrylonitrile (**2e**)*

Yellow solid, 94%; m.p. = 99–101 °C; ^{1}H NMR (300 MHz, $CDCl_3$): δ (ppm): 3.95 (s, 3H, OCH_3), 3.97 (s, 3H, OCH_3), 6.91 (d, J = 8.4 Hz, 1H), 7.10–7.15 (m, 2H), 7.33 (dd, J_1 = 2.1 Hz, J_2 = 8.4 Hz, 1H), 7.38 (s, 1H), 7.60–7.65 (m, 2H), 7.69 (d, J = 2.1 Hz, 1H); ^{13}C NMR (75 MHz, $CDCl_3$): δ (ppm): 55.49 (OCH_3), 55.52 (OCH_3), 107.13 (C), 110.30 (CH), 110.54 (CH), 115.41 (d, $J_{C\text{-}F}$ = 21.7 Hz, 2CH), 118.01 (CN), 123.86 (CH), 126.11 (C), 127.06 (d, $J_{C\text{-}F}$ = 8.2 Hz, 2CH), 130.56 (C), 141.55 (CH), 148.65 (C–O), 150.80 (C–O), 160.82 (d,

$J_{C\text{-}F}$ = 248.2 Hz, CF); ^{19}F NMR (282 MHz, $CDCl_3$): δ (ppm): −112.36 (s, F).

2.2.6. *(Z)-2-(p-fluorophenyl)-3-(thiophen-2-yl)acrylonitrile (**2f**)*

Yellow solid, 75%; m.p. = 98–100 °C; ^{1}H NMR (300 MHz, $CDCl_3$): δ (ppm): 7.12–7.19 (m, 3H), 7.56 (d, J = 5.1 Hz, 1H), 7.60–7.69 (m, 4H); ^{13}C NMR (75 MHz, $CDCl_3$): δ (ppm): 106.77 (C), 115.54 (d, $J_{C\text{-}F}$ = 21.7 Hz, 2CH), 117.50 (CN), 127.00 (d, $J_{C\text{-}F}$ = 8.2 Hz, 2CH), 127.38 (CH), 129.57 (CH), 129.63 (d, $J_{C\text{-}F}$ = 3 Hz, C), 131.84 (CH), 133.59 (d, $J_{C\text{-}F}$ = 1.5 Hz, CH), 137.29 (C), 160.92 (d, $J_{C\text{-}F}$ = 248.2 Hz, CF); ^{19}F NMR (282 MHz, $CDCl_3$): δ (ppm): −111.86 Hz (s, F).

2.3. *General procedure for the synthesis of phenanthrene derivatives **P1–6***

α,β-unsaturated nitrile **2** (1.6 mmol, 1 eq) was dissolved in 1 L of toluene. Then 40 mg of iodine (0.16 mmol, 10 mol%) was added to the solution. The mixture was vigorously stirred for approximately 3 h under UV irradiation by a 150 W mercury lamp. After completion of the reaction (CCM analysis), toluene was evaporated. The crude product was purified by flash silica gel column chromatography using cyclohexane/EtOAc (90/10) as the eluent. Spectral data and physical characteristics are given below for each phenanthrene derivative.

2.3.1. *6-fluoro-3-methoxyphenanthrene-9-carbonitrile (**P1**)*

White solid, 78%; m.p. = 225–227 °C; ^{1}H NMR (300 MHz, $CDCl_3$): δ (ppm): 4.06 (s, 3H, OCH_3), 7.31 (dd, J_1 = 2.4 Hz, J_2 = 9 Hz, 1H), 7.46 (td, J_1 = 2.4 Hz, J_2 = 9 Hz, 1H), 7.84–7.87 (m, 2H), 8.14 (s, 1H), 8.18 (dd, J_1 = 2.4 Hz, J_2 = 10.8 Hz, 1H), 8.24 (dd, J_1 = 5.7 Hz, J_2 = 9 Hz, 1H); ^{13}C NMR (75 MHz, $CDCl_3$): δ (ppm): 55.66 (OCH_3), 104.33 (CH), 106.21 (C), 108.28 (d, $J_{C\text{-}F}$ = 22.5 Hz, CH); 117.11 (d, $J_{C\text{-}F}$ = 23.2 Hz, CH), 118.06 (CN), 118.56 (CH); 124.7 (C), 126.01 (C), 128.42 (d, $J_{C\text{-}F}$ = 9 Hz, CH), 131.18 (CH), 131.22 (C), 132.94 (C), 134.47 (CH), 160.40 (d, $J_{C\text{-}F}$ = 246.7 Hz, CF), 161.02 (C–O); ^{19}F NMR (282 MHz, $CDCl_3$): δ (ppm): −111.33 (s, F); IR: ν (cm^{-1}): 3036, 2983, 2216 (CN), 1521, 1503, 1476, 1454, 1421, 1381, 1363, 1273, 1230, 1215, 1181, 1139, 1100, 1020, 952, 898, 855, 837, 808, 722, 689, 639, 563, 552, 480, 427.

2.3.2. *3-bromo-6-fluorophenanthrene-9-carbonitrile (**P2**)*

White solid, 97%; m.p. = 247–249 °C; ^{1}H NMR (300 MHz, $CDCl_3$): δ (ppm): 7.53–7.60 (m, 1H), 7.84 (s, 2H), 8.19 (s, 1H), 8.24 (dd, J_1 = 2.4 Hz, J_2 = 10.2 Hz, 1H), 8.31 (dd, J_1 = 5.7 Hz, J_2 = 9 Hz, 1H), 8.72 (s, 1H); ^{13}C NMR (75 MHz, $CDCl_3$): δ (ppm): 108.50 (d, $J_{C\text{-}F}$ = 23.2, CH), 109.55 (C), 117.35 (CN), 117.80 (d, $J_{C\text{-}F}$ = 23.8 Hz, CH), 122.52 (C), 124.73 (C), 126.12 (CH), 128.60 (d, $J_{C\text{-}F}$ = 9 Hz, CH), 128.65 (C), 130.76 (C), 130.87 (CH), 131.69 (CH), 132.43 (C), 134.04 (CH); 160.86 (d, $J_{C\text{-}F}$ = 246.7 Hz, CF); ^{19}F NMR (282 MHz, $CDCl_3$): δ (ppm): −109.50 (s, F); IR: ν (cm^{-1}): 3076, 2919, 2850, 2215 (CN), 1621, 1581, 1517, 1488, 1424, 1406, 1324, 1266, 1203, 1179, 1145, 1063, 1022, 917, 903, 859, 818, 807, 715, 670, 635, 535, 488, 467, 425, 411.

2.3.3. *6-fluorophenanthrene-3,9-dicarbonitrile (**P3**)*

White solid, 92%; m.p. = 245–247 °C; ^{1}H NMR (300 MHz, DMSO-d_6): δ (ppm): 7.82–7.84 (m, 1H), 8.13–8.29 (m, 3H), 8.72 (s, 1H), 8.92–8.94 (m, 1H), 9.49 (s, 1H); ^{13}C NMR (75 MHz, DMSO-d_6): δ (ppm): 109.90 (d, $J_{C\text{-}F}$ = 21 Hz, CH), 110.74 (C), 112.43 (C), 118.40 (d, $J_{C\text{-}F}$ = 22.5 Hz, CH), 118.44 (CN), 118.57 (CN), 125.26 (C), 128.23 (d, $J_{C\text{-}F}$ = 8.2 Hz, CH), 129.54 (CH), 129.90 (CH), 130.81 (CH), 131.13 (C), 131.88 (C), 132.00 (C), 134.67 (CH), 161.17 (d, $J_{C\text{-}F}$ = 249.7 Hz, CF); ^{19}F NMR (282 MHz, $CDCl_3$): δ (ppm): −109.14 (s, F); IR: ν (cm^{-1}): 3071, 2919, 2227 (CN), 2218 (CN), 1620, 1600, 1524, 1504, 1451, 1418, 1392, 1363, 1333, 1275, 1216, 1180, 1139, 1112, 1022, 952, 904, 875, 857, 838, 813, 725, 691, 644, 567, 552, 534, 488, 424.

2.3.4. *3,6-difluorophenanthrene-9-carbonitrile (**P4**)*

Yellow solid, 88%; m.p. = 217–219 °C; ^{1}H NMR (300 MHz, $CDCl_3$): δ (ppm): 7.44–7.55 (m, 2H), 7.92 (dd, J_1 = 6 Hz, J_2 = 8.7 Hz, 1H), 8.11–8.17 (m, 3H), 8.26 (dd, J_1 = 5.7 Hz, J_2 = 8.7 Hz, 1H); ^{13}C NMR (75 MHz, $CDCl_3$): δ (ppm): 107.94 (d, $J_{C\text{-}F}$ = 23.2 Hz, CH), 108.07 (d, $J_{C\text{-}F}$ = 22.5 Hz, CH), 116.97 (CN), 117.00 (d, $J_{C\text{-}F}$ = 23.2 Hz, CH), 117.27 (d, $J_{C\text{-}F}$ = 23.5 Hz, CH), 125.24 (2C), 126.35 (2C), 128.08 (d, $J_{C\text{-}F}$ = 8.2 Hz, CH), 131.42 (d, $J_{C\text{-}F}$ = 9.7 Hz, CH), 133.55 (CH), 160.15 (d, $J_{C\text{-}F}$ = 249 Hz, CF), 161.20 (d, $J_{C\text{-}F}$ = 249.7 Hz, CF); ^{19}F NMR (282 MHz, $CDCl_3$): δ (ppm): −107.70 (s, F); −110.03 (s, F); IR: ν (cm^{-1}): 3076, 2983, 2215 (CN), 1620, 1597, 1523, 1507, 1472,

1449, 1426, 1387, 1364, 1274, 1229, 1218, 1202, 1172, 1142, 1104, 1032, 1020, 967, 956, 902, 857, 849, 838, 815, 728, 693, 644, 606, 564, 553, 482, 463, 429.

2.3.5. *6-fluoro-2,3-dimethoxyphenanthrene-9-carbonitrile (P5)*

White solid, 70%; m.p. = 237–239 °C; ^{1}H NMR (300 MHz, $CDCl_3$): δ (ppm): 4.08 (s, 3H, OCH_3), 4.15 (s, 3H, OCH_3), 7.24 (s, 1H), 7.44 (td, J_1 = 1.2 Hz, J_2 = 9 Hz, 1H, H_7), 7.78 (s, 1H), 8.09 (s, 1H), 8.10 (dd, J_1 = 1.2 Hz, J_2 = 11.4 Hz, 1H, H_5), 8.23 (dd, J_1 = 6 Hz, J_2 = 8.7 Hz, 1H, H_8); ^{13}C NMR (75 MHz, $CDCl_3$): δ (ppm): 56.17 (OCH_3), 56.21 (OCH_3), 103.17 (CH), 106.71 (C), 107.60 (d, $J_{C\text{-}F}$ = 22.5 Hz, CH), 108.63 (CH), 116.20 (d, $J_{C\text{-}F}$ = 24 Hz, CH), 118.16 (CN), 125.17 (C), 125.37 (C), 126.51 (C), 128.45 (d, J = 9 Hz, CH), 130.96 (d, $J_{C\text{-}F}$ = 9 Hz, C), 133.53 (CH), 150.49 (C–O), 151.87 (C–O), 160.35 (d, $J_{C\text{-}F}$ = 246 Hz, CF); ^{19}F NMR (282 MHz, $CDCl_3$): −111.41 (s, F); IR: ν (cm^{-1}): 3082, 3006, 2925, 2838, 2215 (CN), 1616, 1525, 1509, 1472, 1418, 1373, 1259, 1213, 1160, 1115, 1037, 1024, 995, 908, 899, 853, 836, 817, 807, 767, 758, 718, 646, 614, 586, 497, 478, 423, 413.

2.3.6. *6-fluoronaphto[2,1-b]thiophene-9-carbonitrile (P6)*

White solid, 65%; m.p. = 224–226 °C; ^{1}H NMR (300 MHz, $CDCl_3$): δ (ppm): 7.36 (td, J_1 = 2.4 Hz, J_2 = 9 Hz, 1H, H_6), 7.78 (d, J = 5.4 Hz, 1H, H_2 or H_3), 7.85 (d, J = 5.4 Hz, 1H, H_3 or H_2), 7.88 (dd, J_1 = 2.4 Hz, J_2 = 9.6 Hz, 1H, H_4), 8.23 (s, 1H, H_9), 8.25 (dd, J_1 = 5.4 Hz, J_2 = 9 Hz, 1H, H_7); ^{13}C NMR (75 MHz, $CDCl_3$): δ (ppm): 106.12 (C), 108.17 (d, $J_{C\text{-}F}$ = 22.5 Hz, CH), 116.41 (d, $J_{C\text{-}F}$ = 24.7 Hz, CH), 117.43 (CN), 121.83 (CH), 125.49 (C), 126.82 (CH), 128.05 (d, $J_{C\text{-}F}$ = 9 Hz, CH), 129.51 (d, $J_{C\text{-}F}$ = 9.7 Hz, C), 130.61 (CH), 135.71 (C), 138.28 (C), 159.71 (d, $J_{C\text{-}F}$ = 249 Hz, CF); ^{19}F NMR (282 MHz, $CDCl_3$): δ (ppm): −110.46 (s, F); IR: ν (cm^{-1}): 3111, 3084, 2215 (CN), 1622, 1510, 1464, 1423, 1371, 1324, 1303, 1261, 1224, 1203, 1188, 1146, 1099, 1051, 968, 884, 858, 847, 811, 769, 728, 708, 667, 615, 564, 485, 459.

3. Results and discussion

In this work, the synthetic approach followed for the construction of tricyclic architectures was based on the oxidative photocyclization reaction of suitably functionalized olefins. First, p-fluorophenylacetonitrile (**1**) was reacted with different commercially available aromatic aldehydes according to a Knoevenagel reaction, producing α,β-unsaturated nitriles **2a–f** with (*Z*)-configuration in 65–94% yields (Scheme 1 and Table 1). The resulting nitriles are well soluble in different organic solvents including toluene, acetone, dichloromethane, chloroform, and ethyl acetate.

Table 1. Chemical yields of α,β-unsaturated nitriles **2a–e**

Compound	R_1	R_2	Aspect	Yield (%)[a]
2a	OMe	H	White solid	85
2b	Br	H	Yellow solid	80
2c	CN	H	White solid	65
2d	F	H	White solid	90
2e	OMe	OMe	Yellow solid	94

[a] Isolated yields.

Table 2. Chemical yields of phenanthrene derivatives **P1–5**

Compound	R_1	R_2	Aspect	Yield (%)[a]
P1	OMe	H	White solid	78
P2	Br	H	White solid	97
P3	CN	H	White solid	92
P4	F	H	Yellow solid	88
P5	OMe	OMe	White solid	70

[a] Isolated yields.

p-Fluorophenylacetonitrile (**1**) was also reacted with 2-thiophene carbaldehyde under the same conditions. This provided **2f** in 75% yield as a yellow solid (Scheme 2).

Fluorinated α,β-unsaturated nitriles **2a–f** were then irradiated with a 150 W mercury lamp, through a Pyrex glass jacket, in toluene for approximately 3 h in the presence of a catalytic amount of iodine as an oxidizing agent. Unfortunately, this reaction conducted on a 500 mg scale per run provided only the desired fluorinated phenanthrene derivatives **P1–5** in 70–97% yields (Scheme 3 and Table 2). It is worth noting that the photo-irradiation conditions are compatible with the different functionalities grafted on the target tricyclic compounds. No photodimer was observed during the photocycliza-

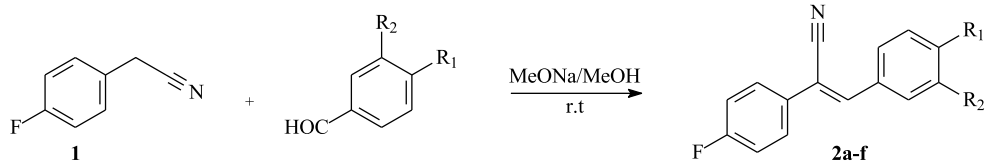

Scheme 1. Synthesis of α,β-unsaturated nitriles **2a–f**.

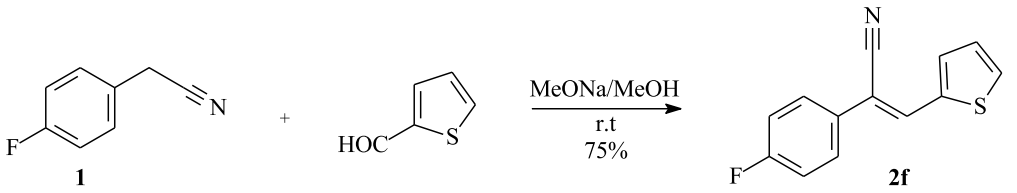

Scheme 2. Synthesis of compound **2f**.

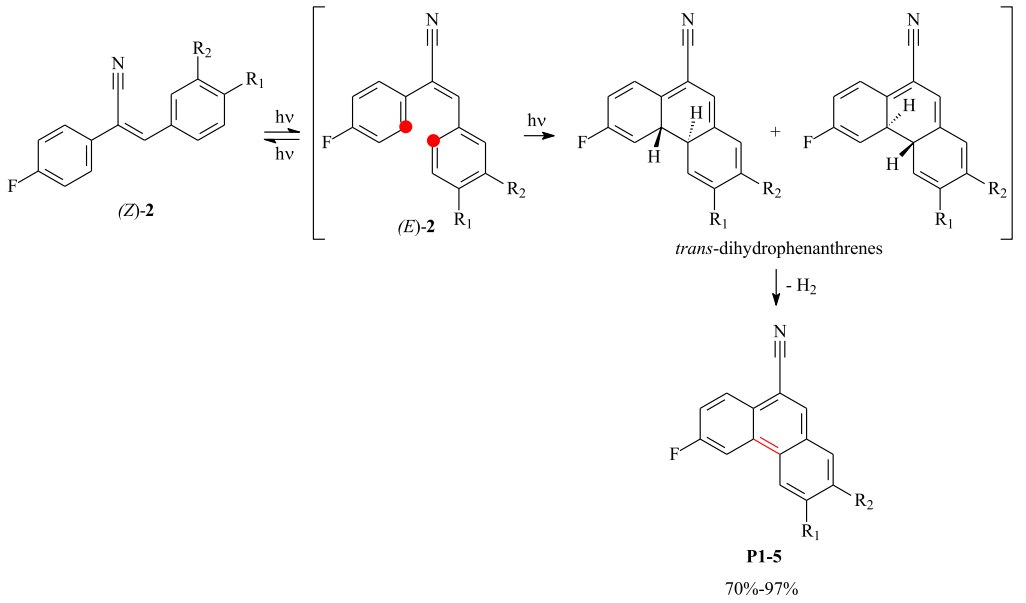

Scheme 3. Photocyclization of α,β-unsaturated nitriles into phenanthrenes **P1–5**.

tion step. The whole photocyclodehydrogenation reaction proceeded via isomerization of (*Z*)-**2** to (*E*)-**2** followed by intramolecular electrocyclization leading to *trans*-dihydrophenanthrenes, which were oxidized to phenanthrene derivatives.

The phenanthrene derivatives were characterized by NMR spectroscopy. For example, the proton NMR spectrum of compound **P5** (Figure 2) displayed three characteristic singlets at 7.24, 7.78, and 8.09 ppm, which were attributed to protons H_1, H_4, and H_{10}. A triplet of doublets (J_1 = 1.2 Hz, J_2 = 9 Hz) was observed at δ = 7.44 ppm, which is typical of proton H_7.

We investigated the ^{1}H–^{1}H COSY NMR spectrum of **P5** (Figure 3) to provide more structural information. Two doublets of doublets at 8.10 ppm (J_1 = 1.2 Hz, J_2 = 11.4 Hz) and 8.23 ppm (J_1 = 6 Hz, J_2 = 8.7 Hz) are attributed to H_5 and H_8, respectively, which couple with H_7.

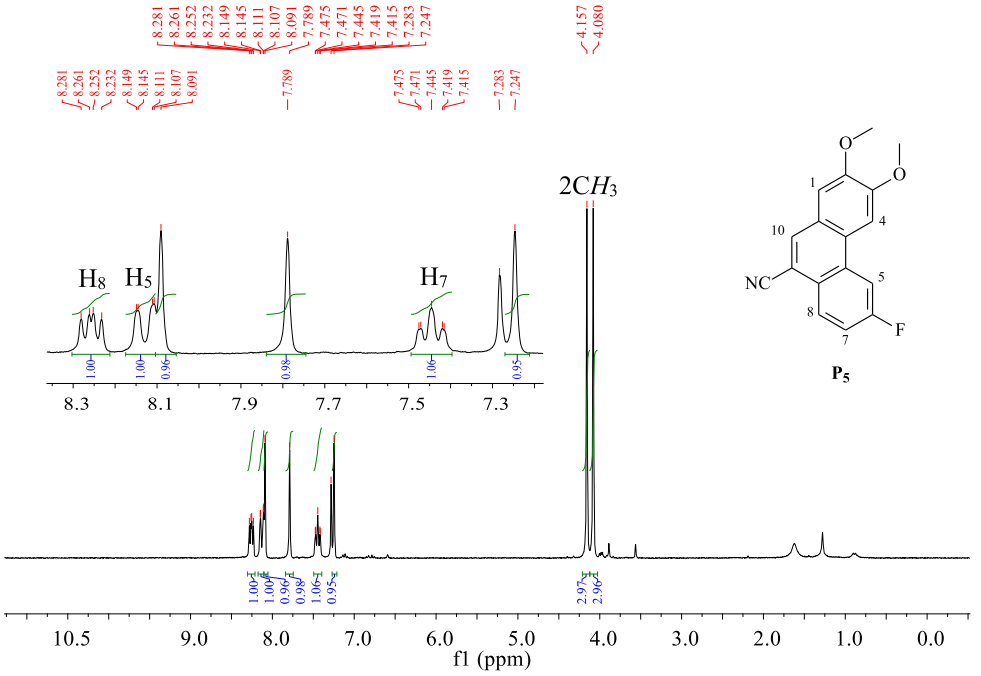

Figure 2. ^{1}H NMR spectrum ($CDCl_3$, 300 MHz, 298 K) of compound **P5**.

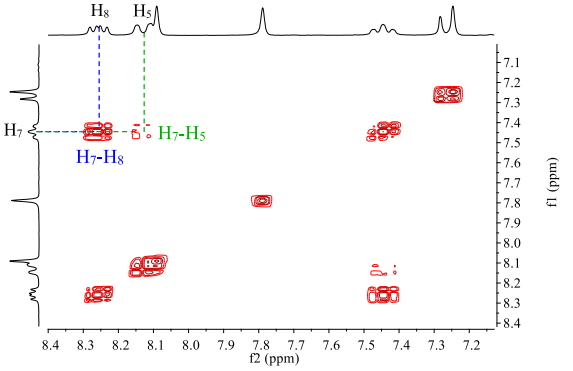

Figure 3. ^{1}H–^{1}H COSY NMR spectrum ($CDCl_3$, 300 MHz, 298 K) of compound **P5**.

The photo-irradiation of the α,β-unsaturated nitrile **2f**, conducted under the same conditions, provided 5-fluoronaphto[2,1-*b*]thiophene-8-carbonitrile **P6** as a white solid in 65% yield (Scheme 4).

The proton NMR spectrum (Figure 4) of compound **P6** shows a triplet of doublets at 7.36 ppm (J_1 = 2.4 Hz, J_2 = 9 Hz) attributed to proton H_6. Two doublets at 7.78 ppm (J = 5.4 Hz) and 7.85 ppm (J = 5.4 Hz) relative to H_2 and H_3 and a singlet at 8.23 ppm, which is typical of proton H_9, are observed.

By using ^{1}H-^{1}H COSY NMR spectroscopy, it is possible to differentiate the peaks for protons H_4 and H_7. In Figure 5, the H_4 signal is located at 7.88 ppm as a doublet of doublets (J_1 = 2.4 Hz, J_2 = 9.6 Hz), while the H_7 signal is overlapped with the H_9 proton signal and is found at 8.23 ppm (J_1 = 5.4 Hz, J_2 = 9 Hz).

UV–Vis spectra of the synthesized α,β-unsaturated nitriles **2a–f** were recorded in chloroform solutions ($C \approx 3 \times 10^{-5}$ mol·L^{-1}) at room temperature. As seen in Figure 6, the UV–Vis spectra of **2a–f** display several absorption bands below 275 nm (256, 263, and 270 nm) with slightly different absorption coefficients (64000–82000 M^{-1}·cm^{-1}) as indicated in Table 3. They are accompanied by one broad absorption band in the low-energy region ($\Delta\lambda$ > 65 nm). These absorption bands are characteristic of π–π* and n–π* transitions. By examining the low-energy region, it is clear that **2d** shows the strongest absorption band at 315 nm ($\varepsilon = 3.89 \times 10^4$ M^{-1}·cm^{-1}), **2c** displays a weaker

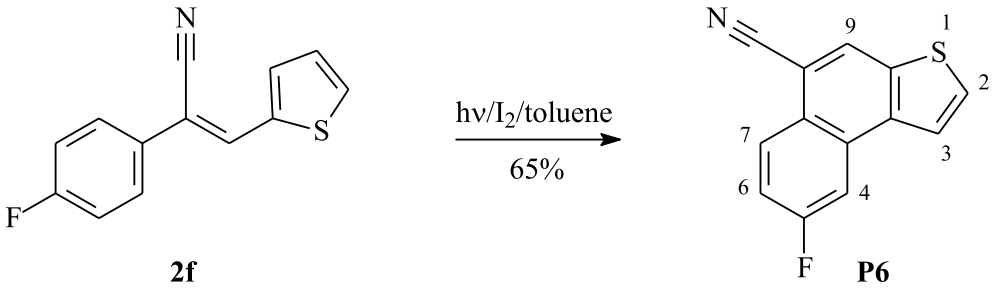

Scheme 4. Synthesis of 5-fluoronaphto[2,1-*b*]thiophene-8-carbonitrile **P6**.

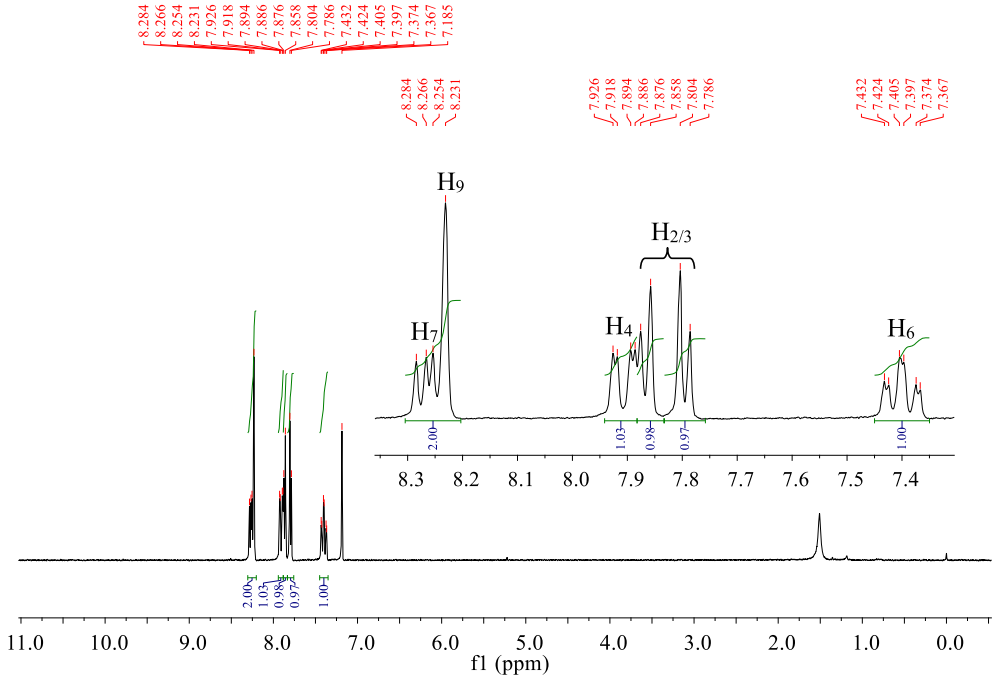

Figure 4. ^{1}H NMR spectrum ($CDCl_3$, 300 MHz, 298 K) of compound **P6**.

band at 322 nm (ε = 1.21 × 10^4 M^{-1}·cm^{-1}), and **2e** exhibits the longest band at 349 nm (the molar extinction coefficient is more than twice as high as that for **2c**). Moving from **2a** to **2e**, the addition of a methoxy group induces a bathochromic shift of 12 nm for the low-energy band (centered at 337 nm) with a slight decrease in the absorption intensity ($\Delta\varepsilon \approx 2400$ M^{-1}·cm^{-1}). From **2d** to **2b**, replacing the fluorine atom by a bromine atom results in a significant decrease in the absorption intensity for the band located between 277 and 367 nm. It appears that the α,β-unsaturated nitriles with electron donor substituents (e.g., methoxy group) on the benzene ring (**2a** and **2e**) or with thiophene nuclei (**2f**) shift the low-energy (>300 nm) absorption maxima to higher wavelengths. The α,β-unsaturated nitriles with electron-withdrawing substituents (e.g. cyano, fluoro, and bromo groups) (**2b**, **2c**, and **2d**) shift the low-energy (>300 nm) absorption maxima to lower wavelengths. The electron-donating substituents lead to a bathochromic shift of the absorption maxima at longer wavelengths between 377 and 400 nm. Electron-withdrawing substituents lead to hypsochromic shifts. The optical band gap energy ($E_{g\text{-}op}$)

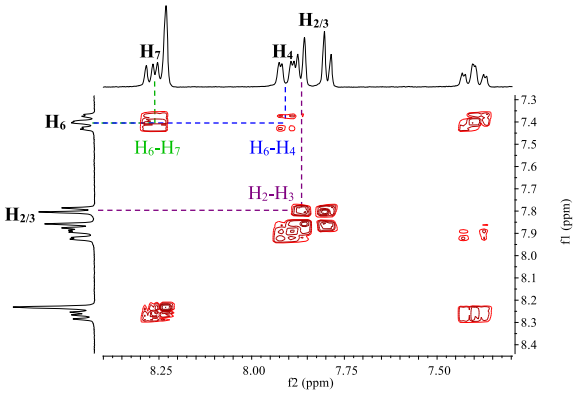

Figure 5. ^{1}H-^{1}H COSY NMR spectrum ($CDCl_3$, 300 MHz, 298 K) of compound **P6**.

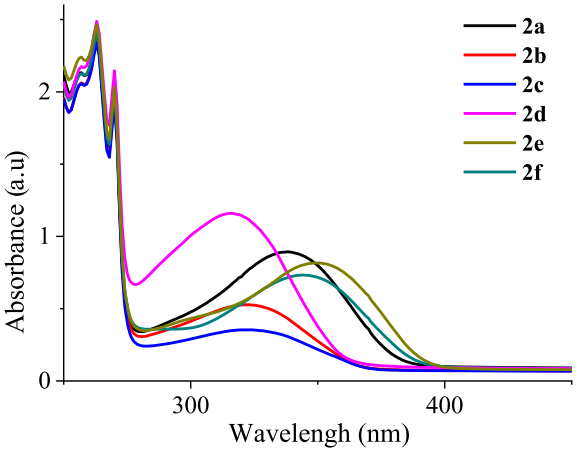

Figure 6. Electronic UV–Vis absorption spectra of α,β-unsaturated nitriles **2a–f** in chloroform solutions ($C \approx 3 \times 10^{-5}$ M).

of each α,β-unsaturated nitrile has been estimated according to the empirical formula

$$E_{\text{g-op}} = hc/\lambda_{\text{onset}},$$
$$E_{\text{g-op}}\ (\text{eV}) = 1240/\lambda_{\text{onset}}.$$

Here h represents the Planck constant ($6.62607004 \times 10^{-34}$ m^2·kg/s), c is the speed of light (3×10^8 m/s), and λ_{onset} is the onset wavelength.

The photocyclization of the α,β-unsaturated nitriles into the corresponding phenanthrene derivatives leads to significant modifications in their absorption spectra by the appearance of new bands between 275 and 400 nm. The photophysical properties of compounds **P1–6** are then examined in

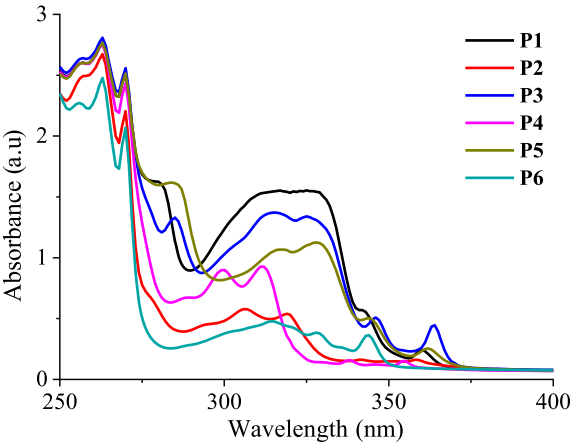

Figure 7. Electronic UV–Vis absorption spectra of phenanthrene derivatives **P1–6** in chloroform solutions ($C \approx 3 \times 10^{-5}$ M).

chloroform solutions ($C \approx 3 \times 10^{-5}$ mol·L^{-1}) at room temperature. These are displayed in Figure 7. The absorption spectra of these compounds show similar features including three intense bands located between 250 and 275 nm ($\varepsilon \sim 69200$–93900 M^{-1}·cm^{-1}) and a shoulder peak around 275 nm followed by several less intense bands up to 380 nm (Table 4). The weaker absorption bands are observed in the low-energy region with intensities in the range 5100–18000 M^{-1}·cm^{-1}. Moving from **P1** to **P5**, the presence of a second methoxy group induces a bathochromic shift of approximately 2–5 nm for the absorption maxima at 275–375 nm with a significant decrease in intensities for the bands at 316 and 327 nm in the range 14300–16100 M^{-1}·cm^{-1}. Compared to **P4**, the bromine atom in **P2** induces a bathochromic shift of approximately 3–8 nm for the bands at 299, 311, 338, and 354 nm. The absorption bands of **P2** below 316 nm are less intense than those of **P4**, but above 316 nm, they become slightly more intense. The optical band gap energy ($E_{\text{g-op}}$) of each α,β-unsaturated nitrile is calculated, and the results are summarized in Table 4.

The PL spectra of phenanthrene derivatives **P1–6** are recorded in chloroform solutions ($C \sim 10^{-5}$ mol·L^{-1}) at room temperature (Figure 8). Compounds **P1–5** exhibit structured emissions displaying several bands at different intensities (Table 5). The difluorinated compound **P4** shows an maximum emission at 353 nm followed

Table 3. Electronic UV–Vis absorption properties of the α,β-unsaturated nitriles **2a–f** in chloroform solutions

Compound	λ_{abs} [a]/nm ($\varepsilon/10^4$ $M^{-1}\cdot cm^{-1}$)[b]	λ_{onset} (nm)	$E_{g\text{-}op}$ [c] (eV)
2a	256 (7.11), 263 (8.02), 270 (6.58), 337 (2.99)	395	3.13
2b	256 (6.88), 263 (7.87), 270 (6.46), 321 (1.71)	377	3.28
2c	256 (6.88), 263 (7.84), 270 (6.46), 322 (1.21)	377	3.28
2d	256 (7.26), 263 (8.26), 270 (7.11), 315 (3.89)	374	3.31
2e	256 (7.45), 263 (8.26), 270 (6.77), 349 (2.75)	398	3.11
2f	256 (7.11), 263 (8.02), 270 (6.58), 343 (2.46)	395	3.13

[a] Absorption maxima measured in $CHCl_3$ solution (3×10^{-5} mol·L^{-1}) at room temperature.

[b] Calculated using the Beer–Lambert law ($\varepsilon = A/lC$), where A = absorbance at λ_{abs}, l = path length (1 cm), and C = concentration in mol·L^{-1}.

[c] The optical band gap ($E_{g\text{-}op}$) was estimated from the onset point of the absorption spectrum: $E_{g\text{-}op} = 1240/\lambda_{onset}$.

Table 4. Electronic UV–Vis absorption properties of phenanthrene derivatives **P1–6** in chloroform solutions

Compound	λ_{abs} [a]/nm ($\varepsilon/10^4$ $M^{-1}\cdot cm^{-1}$)[b]	λ_{onset} (nm)	$E_{g\text{-}op}$ [d] (eV)
P1	256 (8.79), 263 (9.39), 270 (8.55), 280 (5.44), 315 (5.19), 326 (5.19), 342 (1.8), 360[c] (0.80)	371	3.34
P2	257 (8.34), 263 (8.97), 270 (7.35), 306 (1.96), 319 (1.82), 341 (0.56), 358[c] (0.54)	378	3.28
P3	256 (8.79), 263 (9.39), 270 (8.55), 285 (4.46), 315 (4.61), 325 (4.51), 345 (1.72), 363[c] (1.48)	378	3.28
P4	256 (8.66), 263 (9.19), 270 (8.07), 288 (2.27), 299 (3.02), 311 (3.09), 338, (0.53), 353[c] (0.51)	358	3.46
P5	256 (8.68), 263 (9.24), 269 (8.37), 284 (5.42), 317 (3.58), 328 (3.76), 344 (1.71), 362[c] (0.86)	378	3.28
P6	256 (7.59), 263 (8.27), 270 (6.92), 301 (1.31), 314 (1.58), 328 (1.28), 343[c] (1.21)	355	3.49

[a] Absorption maxima measured in chloroform ($C \approx 3 \times 10^{-5}$ mol·L^{-1}) at room temperature.

[b] Calculated using the Beer–Lambert law ($\varepsilon = A/lC$), where A = absorbance at λ_{abs}, l = path length (1 cm), and C = concentration in mol·L^{-1}.

[c] First absorption maxima (λ_{1abs}).

[d] The optical band gap ($E_{g\text{-}op}$) was estimated from the onset point of the absorption spectrum: $E_{g\text{-}op} = 1240/\lambda_{onset}$.

by three other bands (369, 375, and 392 nm) that are less intense and a shoulder peak at 415 nm. The phenanthrene-like derivative **P6** exhibits an emission with three bands at 348, 362, and 381 nm and one shoulder peak at 398 nm. The maximum emission of **P6** (λ_{ems} = 362 nm) is shifted to the highest wavelengths with 7 nm, in comparison to that of **P4** (λ_{ems} = 353 nm). The emission spectrum of **P2** shows the same signature as that of **P4**, including three emission bands (359, 376, and 397 nm) and a shoulder peak (415 nm) with enhanced intensities and are shifted to the highest wavelengths with 11–14 nm. Unlike the previous compounds, **P5** shows two emission bands at 366 and 383 nm followed by a shoulder peak located at 400 nm, the first of which is the most intense. **P1** exhibits two emission bands at 361 and 399 nm with almost the same intensities and a shoulder peak at 417 nm. Finally, the emission spectrum of compound **P3** is totally different. It is shifted more to the highest wavelengths (red-shifted) than the others since it displays an emission at 437 nm and a shoulder peak at 450 nm. The destructured profile as well

Table 5. Photoluminescence properties of phenanthrene derivatives **P1–6** in chloroform. Stokes shifts are calculated in wavelength and wavenumber units

Compound	Photoluminescence		Stokes shift	
	λ_{ems} [a] (nm)	FWHM[d] (nm)	λ_{ems}^{max}–λ_{1abs} (nm)	$\Delta\nu$ (cm^{-1})
P1	361, 379[c], 399, 417[b]	49	19	1392
P2	359, 376[c], 397, 415[b]	30	18	1337
P3	437[c], 450[b]	31	74	4664
P4	353[c], 369, 375, 392, 415	47	0	0
P5	366[c], 383, 400[b]	36	5	378
P6	348, 362[c], 381, 398[b]	25	19	1530

[a] Emission measured in chloroform ($C \approx 10^{-5}$ mol·L^{-1}) at room temperature; fluorescence excitation at 350 nm.

[b] Shoulder peak.

[c] Maximum emission (λ_{ems}^{max}).

[d] Spectrum full width at half maximum.

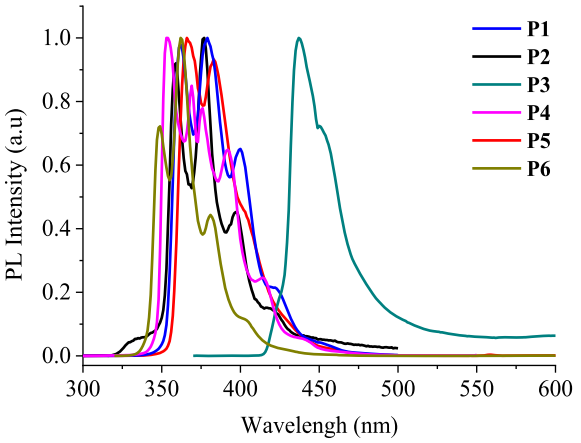

Figure 8. Normalized emission spectra (λ_{exc} = 350 nm) of phenanthrene derivatives **P1–6** measured in chloroform solutions ($C \sim 10^{-5}$ mol·L^{-1}).

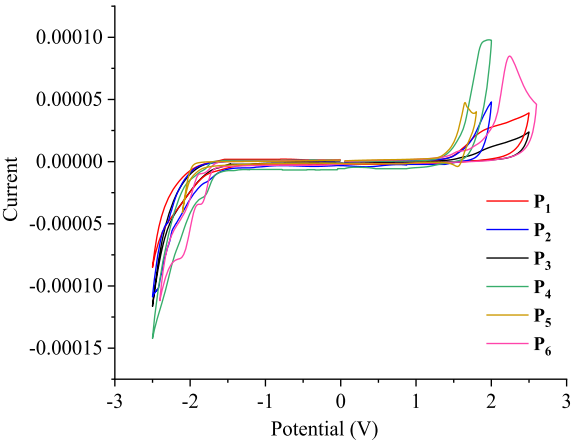

Figure 9. Cyclic voltammograms of **P1–6** registered in 0.1 M nBu$_4$NPF$_6$/CH$_2$Cl$_2$ at a scan rate of 50 mV/s.

as the bathochromic shift of this emission illustrates the intense character of the charge transfer within the molecule **P3** in the excited state.

The electrochemical behaviors of the phenanthrene derivatives **P1–6** are evaluated using cyclic voltammetry (CV) in dichloromethane with nBu$_4$NPF$_6$ (0.1 M) as the supporting electrolyte versus the SCE. As shown in Figure 9, the cyclic voltammograms, recorded at a scanning rate of 50 mV/s, indicate that compounds **P1–6** exhibit irreversible anodic and cathodic peaks. Analysis of responses in CV allowed the determination of the oxidation potentials, which were found to be 1.42, 1.48, 1.46, 1.55, 1.28, and 1.64 V, versus the SCE. In addition, the reduction potentials were −1.67, −1.60, −1.59, −1.63, −1.75, and −1.67 V for **P1–6**, respectively.

An empirical method [26,27] was then utilized to examine the highest occupied molecular orbital (HOMO) and the lowest unoccupied molecular or-

Table 6. Electrochemical onset potentials and electronic energy levels of **P1–6**

Compound	$V_{\text{onset-ox}}$ (V)	$V_{\text{onset-red}}$ (V)	E_{HOMO} (eV)	E_{LUMO} (eV)	$E_{\text{g-el}}$ (eV)
P1	1.42	−1.67	−5.72	−2.63	3.09
P2	1.48	−1.60	−5.78	−2.70	3.08
P3	1.46	−1.59	−5.76	−2.71	3.05
P4	1.55	−1.63	−5.85	−2.67	3.18
P5	1.28	−1.75	−5.58	−2.55	3.03
P6	1.64	−1.67	−5.94	−2.63	3.31

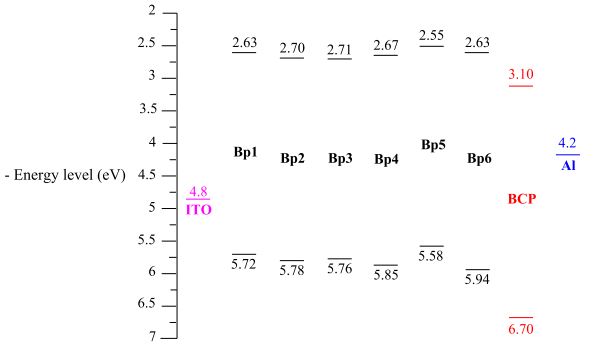

Figure 10. Comparison of the HOMO–LUMO energy levels of **P1–6** and those of BCP, indium tin oxide (ITO), and aluminum.

bital (LUMO) energy levels as well as the electrochemical band gap ($E_{\text{g-el}}$) as follows:

- E_{HOMO} (IP, ionization potential) = $-(V_{\text{onset-ox}} - V_{\text{FOC}} + 4.8)$
- E_{LUMO} (EA, electron affinity) = $-(V_{\text{onset-red}} - V_{\text{FOC}} + 4.8)$
- $E_{\text{g-el}} = (E_{\text{LUMO}} - E_{\text{HOMO}})$ eV.

Here the value 4.8 represents the energy level of the ferrocene/ferrocenium couple, V_{FOC} corresponds to the ferrocene half-wave potential (0.50 V), $V_{\text{onset-ox}}$ is the oxidation onset, and $V_{\text{onset-red}}$ is the material reduction onset, all measured versus Ag/AgCl. As shown in Table 6, the calculated electrochemical band gap ($E_{\text{g-el}}$) varies from 3.03 to 3.31 eV.

The difference between the electrochemical and optical band gaps is attributed to the interface barrier between the electrode and each phenanthrene derivative [28,29] and the exciton binding energy. Interestingly, the energy band gap values of the tricyclic units **P1–6** appear to be less than the electrochemical band gap ($E_{\text{g-el}}$ = 3.46 eV) of a benzo[*ghi*]perylene derivative bearing two electron-withdrawing methoxy carbonyl groups, which has been elaborated and used recently for the construction of field-effect transistors [30].

The LUMO levels estimated for systems **P1–6** are as good as that of bathocuproine (BCP), which is extensively used as an electron-injection, hole-blocking layer in OLEDs [31]. It prohibits excitons diffusing toward the Al electrode where they would otherwise be quenched. However, the quick crystallization of BCP reduces the device performance [32,33]. For this reason, it is better to replace BCP by another material in such devices. In fact, **P1–6** might be suitable candidates to play the role of BCP by serving as hole-transport as well as electron-transport layers (Figure 10).

4. Conclusion

In this work, we prepared new functional fluorophenanthrene derivatives through a short synthetic approach under mild conditions by using commercially available and very low cost starting materials. The absorption and the PL properties of the target phenanthrenes were experimentally evaluated in solutions, and significant results were noted. Phenanthrenes **P1**, **2**, and **4**-**6** reveal a blue emission. **P3** shows a red-shifted emission due to an impressive intramolecular charge transfer. The electrochemical behavior of these tricyclic systems was also evaluated, demonstrating a notable charge transfer interaction owing to their π-conjugated electronic system. These properties suggest the application of these compounds as candidates for OLED-like and electroluminescent devices.

Acknowledgment

The authors extend their appreciation to the deanship of scientific research at University of Tabuk for funding this work through research group number RGP S-1440-0315.

References

[1] S. Wang, Z. Cheng, X. Song, X. Yan, K. Ye, Y. Liu, G. Yang, Y. Wang, *Appl. Mater. Interfaces*, 2017, **9**, 9892-9901.
[2] J. Li, G. Hu, N. Wang, T. Hu, Q. Wen, P. Lu, Y. Wang, *J. Org. Chem.*, 2013, **78**, 3001-3008.
[3] R. Liu, J. P. S. Farinha, M. A. Winnik, *Macromolecules*, 1999, **32**, 3957-3963.
[4] Y. Zhang, M. Xiao, N. Su, J. Zhong, H. Tan, Y. Wang, Y. Liu, Y. Pei, R. Yang, W. Zhu, *Org. Electron.*, 2014, **15**, 1173-1183.
[5] J. Huang, B. Xiao, J. Wang, Y. Wang, X. Peng, X. Miao, Q. Pan, Y. Mo, W. Deng, H. Wu, Y. Cao, *Org. Electron.*, 2014, **15**, 2311-2321.
[6] X. Ouyang, X.-L. Li, X. Zhang, A. Islam, Z. Ge, S.-J. Su, *Dyes Pigm.*, 2015, **122**, 264-271.
[7] M. Dadsetani, A. Ebrahimian, H. Nejatipour, *Mater. Sci. Semicond. Process.*, 2015, **34**, 236-245.
[8] Y. Yuan, D. Li, X. Zhang, X. Zhao, Y. Liu, J. Zhang, Y. Wang, *New J. Chem.*, 2011, **35**, 1534-1540.
[9] Y. Zhang, S.-L. Lai, Q.-X. Tong, M.-F. Lo, T.-W. Ng, M.-Y. Chan, Z.-C. Wen, J. He, K.-S. Jeff, X.-L. Tang, W. Liu, C. Ko, P. Wang, C. Lee, *Chem. Mater.*, 2011, **24**, 61-70.
[10] G. Y. Sang, Y. P. Zou, Y. F. Li, *J. Phys. Chem. C*, 2008, **112**, 12058-12064.
[11] S. H. Park, Y. Jin, J. Y. Kim, S. H. Kim, J. Kim, H. Suh, K. Lee, *Adv. Funct. Mater*, 2007, **17**, 3063-3068.
[12] S. Song, Y. Jin, K. Kim, S. H. Kim, Y. B. Shim, K. Lee, H. Suh, *Tetrahedron Lett.*, 2008, **49**, 3582-3587.
[13] H. Suh, Y. Jin, S. H. Park, D. Kim, J. Kim, C. Kim, J. Y. Kim, K. Lee, *Macromolecules*, 2005, **38**, 6285-8589.
[14] J. Shi, H. Wang, D. Song, H. Tian, Y. Geng, D. Yan, *Thin Solid Films*, 2008, **516**, 3270-3273.
[15] B. Hu, C. Yao, X. R. Huang, *Spectrosc. Lett.*, 2012, **45**, 17-21.
[16] H.-W. Hung, N. Yokoyama, M. Yahiro, C. Adachi, *Thin Solid Films*, 2008, **516**, 8717-8720.
[17] J. Li, G. Hu, N. Wang, T. Hu, Q. Wen, P. Lu, Y. Wang, *J. Org. Chem.*, 2013, **78**, 3001-3008.
[18] B. Wang, X. Qiao, Z. Yang, Y. Wang, S. Liu, D. Ma, Q. Wang, *Org. Electron.*, 2018, **59**, 32-38.
[19] Y. Nicolas, P. Blanchard, E. Levillain, M. Allain, N. Mercier, J. Roncali, *Org. Lett.*, 2004, **6**, 273-276.
[20] J. Roncali, P. Frère, P. Blanchard, R. de Bettignies, M. Turbiez, S. Roquet, P. Leriche, Y. Nicolas, *Thin Solid Films*, 2006, **511–512**, 567-575.
[21] R. Mondal, N. Miyaki, H. A. Becerril, J. E. Norton, J. Parmer, A. C. Mayer, M. L. Tang, J. Brédas, M. D. McGehee, Z. Bao, *Chem. Mater.*, 2009, **21**, 3618-3628.
[22] A. L. Pitman, J. A. Mcleod, E. K. Sarbisheh, E. Kurmaev, J. Müller, A. Moewes, *J. Phys. Chem. C*, 2013, **117**, 19616-19621.
[23] X.-W. Yan, Y. Wang, M. Gao, D. Ma, Z. Huang, *J. Phys. Chem*, 2016, **120**, 22565-22570.
[24] X. Zhang, J. Lin, X. Ouyang, Y. Liu, X. Liu, Z. Ge, *J. Photochem. Photobio. A Chem.*, 2013, **268**, 37-43.
[25] S. B. Akula, H.-S. Chen, C. Su, B. Chen, J. Chiou, C. Shieh, Y. Lin, W. Li, *Inorg. Chem.*, 2017, **56**, 12987-12995.
[26] J. Pommerehne, H. Vestweber, W. Guss, R. F. Mahrt, H. Bassler, M. Porsch, J. Daub, *Adv. Mater.*, 1995, **7**, 551-554.
[27] J. L. Bredas, R. Silbey, D. S. Boudreaux, R. R. Chance, *J. Am. Chem. Soc.*, 1983, **105**, 6555-6559.
[28] D. R. T. Zahn, G. N. Gavrila, G. Salvan, *Chem. Rev.*, 2007, **107**, 1161-1232.
[29] D. A. M. Egbe, B. Carbonnier, E. L. Paul, D. Mühlbacher, T. Kietzke, E. Birckner, D. Neher, U.-W. Grummt, T. Pakula, *Macromolecules*, 2005, **38**, 6269-6275.
[30] S. Hirayama, H. Sakai, Y. Araki, M. Tanaka, M. Imakawa, T. Wada, T. Takenobu, T. Hasobe, *Chem. Eur. J.*, 2014, **20**, 1-14.
[31] H. Gommans, B. Verreet, B. P. Rand, R. Muller, J. Poortmans, P. Heremans, J. Genoe, *Adv. Funct. Mater.*, 2008, **18**, 3686-3691.
[32] P. Peumans, V. Bulovic, S. R. Forrest, *Appl. Phys. Lett.*, 2000, **76**, 2650-2652.
[33] Z. R. Hong, Z. H. Huang, X. T. Zeng, *Thin Solid Films*, 2007, **515**, 3019-3023.